IEEE Access
Multidisciplinary | Rapid Review | Open Access Journal

Received August 7, 2020, accepted October 4, 2020, date of publication October 19, 2020, date of current version October 30, 2020.

Digital Object Identifier 10.1109/ACCESS.2020.3032279

Imaging Velocity Fields Analysis of Space Camera for Dynamic Circular Scanning

TINGTING XU[1,2,3], XIUBIN YANG[1,3], SHAOEN WANG[1,2,3], JINLIANG HAN[1,2,3], LIN CHANG[1,3], AND WEI YUE[1,2,3]

[1]Key Laboratory of Space-Based Dynamics and Rapid Optical Imaging Technology, Chinese Academy of Sciences, Changchun 130033, China
[2]Daheng College, University of Chinese Academy of Sciences, Beijing 100039, China
[3]Changchun Institute of Optics, Fine Mechanics, and Physics, Chinese Academy of Sciences, Changchun 130033, China

Corresponding author: Xiubin Yang (yangxiubin@ciomp.ac.cn)

This work was supported in part by the National Natural Science Foundation of China (NSFC) under Grant 61705222 and Grant 62005275, and in part by the Major Projects of the Ministry of Science and Technology under Grant 2016YFB0501202.

ABSTRACT Compared with traditional push-broom imaging, the space camera that performs the new circular scanning imaging can effectively enlarge the imaging area and obtain high-resolution images. However, the imaging velocity fields of space camera will seriously deteriorate the image quality in the circular scanning imaging process. And the velocity fields are anisotropically distributed due to various factors, including attitude maneuvering, satellite precession, earth curvature, and earth rotation. Therefore, this paper proposes a mathematical model of the velocity field to analyze the effect of circular scanning imaging. Based on the principle of ray tracing, the expression of the instantaneous velocity field on the ground is first derived, and then the corresponding image velocity field is obtained by mapping the velocity vector to the focal plane. In addition, numerical simulations and image simulations are performed to analyze the anisotropy distribution of the velocity vectors. Moreover, the dynamic characteristics of the space camera are analyzed to evaluate the performance of this new imaging. The simulation results show that the higher velocity leads to worse imaging quality. The study of this paper provides guidance for attitude planning and imaging assessment for new remote sensing imaging of space cameras.

INDEX TERMS Space camera, circular scanning imaging, velocity field, image quality, ray tracing.

I. INTRODUCTION

Optical remote sensing technology has been widely used in majority of military and civilian fields such as environmental monitoring, urban construction, and military reconnaissance. Currently, space optical imaging is an important information acquisition method for acquiring images with detailed optical characteristics. However, due to the limitations of the aperture and focal length of the optical system, images with both high-resolution and wide range are difficult achieved by traditional space optical imaging like push-broom imaging, which limits the practicality of the traditional imaging system [1], [2].

To break through this contradiction, one resolution is large field-of-view (FOV) imaging, which utilizes multiple detectors for stitching to obtain a large ground coverage. This technology has been applied to Gaofen-2, World-View, Pleiades and other agile satellites [3]–[5]. Despite the advantage of this stitching, there are still some issues that deserve attention, for instance, limited area coverage, misalignment of focal plane pixels, increased size, weight, and power consumption of the satellite.

Fortunately, the rapid development of camera imaging capability and satellite maneuverability [6]–[10] has made it possible to design new dynamic imaging modes [11]. For example, Cao *et al.* at Harbin Institute of Technology first proposed a circular scanning imaging mode for space cameras [12]. This mode performs push-broom imaging and rotation imaging simultaneously by tilting the camera on the satellite platform. Compared with stitching imaging, circular scanning imaging effectively enlarges the ground coverage without changing inherent parameters of the imaging system, such as camera focal length and pixel size of the detector. And Cao *et al.* also calculated the maximum rotation velocity of the satellite platform so that the two adjacent frames could be seamlessly stitched. Song *et al.* of our team established the dynamic circular scanning imaging model, analyzed imaging parameters such as the ground pixel resolution (GSD) and the swath [13]. The design of imaging parameters needs to be considered with actual imaging requirements to ensure that it will not affect the imaging quality.

The associate editor coordinating the review of this manuscript and approving it for publication was Datong Liu.

Although the above researchers have proposed the dynamic imaging mode and calculated imaging parameters, they have not analyzed the image quality affected by dynamic characteristics [14]–[16]. One of these characteristics is the changing velocity field, which has a serious impact on the clarity of the image. According to the published literature on the velocity field analysis of space cameras, Huang *et al.* [17] deduced mathematical expressions of changing image velocities through the coordinate transformation method. Wang *et al.* [18] established motion equations of the target and analyzed the distribution of the instantaneous velocity field. However, these models were limited to the traditional push-broom imaging along the orbit with a large attitude angle.

The remainder of this paper is organized as follows. The circular scanning imaging process is analyzed, and a mathematical model of the velocity field is established based on the principles of ray tracing and vector mapping in Section 2. The numerical and image simulations are conducted, and an objective criterion Peak Signal to Noise Ratio (PSNR) is used to analyze the image quality of this imaging in Section 3. Finally, the total research work of this paper is summarized, and the advantages and disadvantages of this imaging mode are discussed in Section 4.

II. MATHEMATICAL MODEL

A. ANALYSIS OF THE CIRCULAR SCANNING IMAGING FOR SPACE CAMERA

The space camera is installed on the satellite platform at an angle η to perform circular scanning. As shown in Fig.1, η is the angle between the optical axis of the camera and the satellite-to-earth axis. Then the camera rotates with the platform while performing conventional push-broom imaging, ensuring the requirement of both high resolution and large width without changing the inherent parameters of satellites, detectors and optical systems [12], [13]. And there is no relative movement between the camera and platform, so that the velocity of the camera is identical to that of platform.

As shown in Fig.1, the circular ground coverage of circular scanning imaging is significantly larger than the striped ground coverage of traditional push-broom imaging, and the ground coverage of a single frame is approximately a trapezoid, the resolution of the target is higher in the inner image. By controlling the rotation velocity of the satellite, the adjacent two frames in the vertical flight direction can be seamlessly stitched, thus achieving a wide coverage imaging within a limited FOV.

Although this circular scanning imaging can greatly enlarge the imaging area, the anisotropic imaging velocity field will have a great impact on imaging, as shown in Fig. 2. The outer image is seriously degraded because the outer velocity is greater than the inner velocity, and the higher the velocity, the lower the image quality. Therefore, it is necessary to establish the mathematical model of the velocity field, analyze the distribution of the instantaneous velocity field and the effect of the dynamic circular scanning imaging.

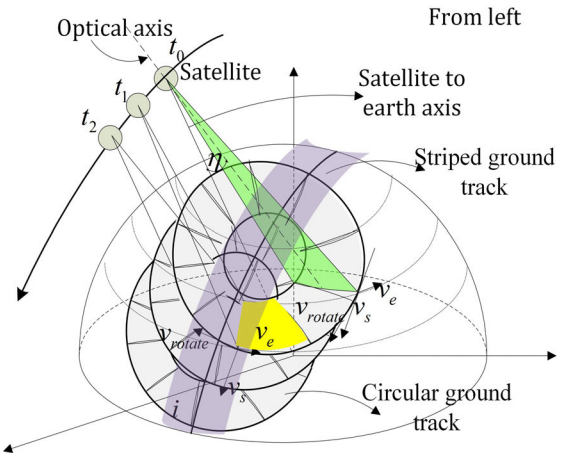

FIGURE 1. Schematic diagram of space camera circular scanning imaging.

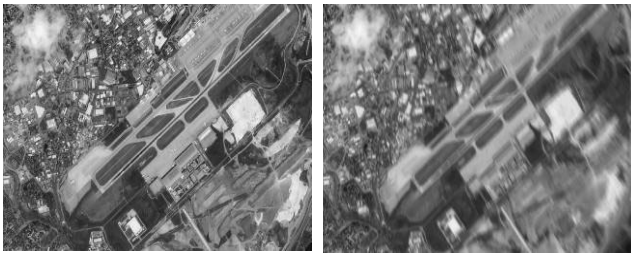

FIGURE 2. Circular scanning imaging image of space camera. (a) Image without rotation; (b) Image with rotation.

B. THE MODELS OF THE INSTANTANEOUS VELOCITY FIELDS

When the space camera performs circular scanning imaging, the target on the ground has three velocities: the projection of orbit precession velocity on the ground v_s; the dynamic rotation velocity v_{rotate} and the linear velocity of earth rotation v_e. Firstly, the dynamic imaging process is analyzed, and then the mathematical models of the instantaneous velocity field on the ground and the image velocity field on the focal plane are established, respectively.

1) ANALYSIS OF THE DYNAMIC IMAGING PROCESS

There are two processes for circular scanning imaging: push-broom imaging along the orbit and rotation imaging. During the rotation imaging process, the optical axis of the camera rotates clockwise at an angular velocity ω_r around the satellite-to-earth axis into a cone, and the fan-shaped expansion of the cone as shown in Fig. 3. In one rotation, the camera rotates σ degree, and the ground track rotates 2π degree. And the rotation angular velocity ω_r is described as:

$$\omega_r = \frac{\sigma}{T} = \frac{2\pi \cdot \sin\eta}{T} \tag{1}$$

where σ can be expressed as: $\sigma = 2\pi \cdot \sin\eta$.

During the process of rotation imaging, the three-axis attitude angles of the satellite platform are θ, φ, ψ and the angular velocities are $\dot{\theta}, \dot{\varphi}, \dot{\psi}$, respectively. The pitch angle and roll angle are unchanged, which ensures the stable imaging

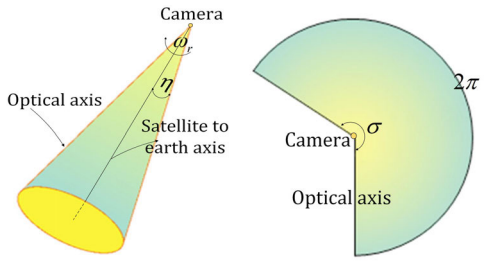

FIGURE 3. The cone area of space camera rotating and its unfolding fan shape.

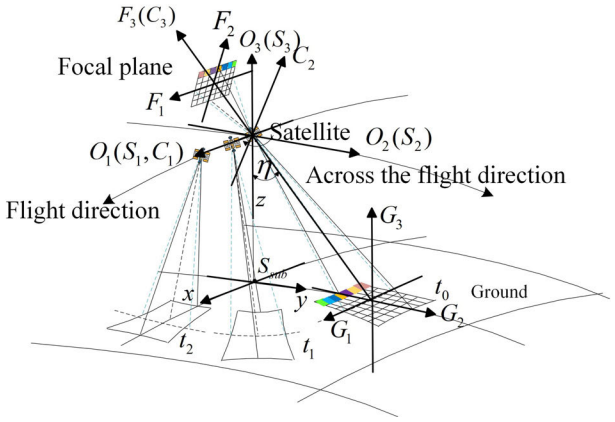

FIGURE 4. The dynamic imaging process of the circular scanning imaging.

of the camera to the ground. And the yaw angle is affected by the rotational motion, which can be expressed as:

$$\psi = \psi_0 + \dot{\psi} \cdot t \tag{2}$$

where ψ_0 is the initial yaw angle of the satellite, the yaw angular velocity $\dot{\psi}$ is ω_r.

As illustrated in Fig. 4, the ray tracing process from targets to pixels contains following five coordinate systems: the ground coordinate system $G(G_1, G_2, G_3)$, the orbit coordinate system $O(O_1, O_2, O_3)$, the satellite coordinate system $S(S_1, S_2, S_3)$, the camera coordinate system $C(C_1, C_2, C_3)$ and the image coordinate system $F(F_1, F_2, F_3)$ [19]. And a simplified coordinate system is established for the calculation of the ground velocity field, which makes the sub-satellite point as a coordinate origin, the flight direction as the x-axis, and the vertical flight direction as the y-axis. During the imaging process of circular scanning imaging, the ground track rotates clockwise from t_0 and the ground coverage in a single frame is a trapezoid. According to the principle of ray tracing, target on the ground is conjugate to pixel on the focal plane.

The imaging of the camera flying along the orbit is the same as the traditional push-broom imaging. At time t_0, the latitude of the sub-satellite point S_{sub} is δ_s, then at time t, the latitude δ_s' can be calculated as:

$$\delta_s' = \arcsin(\sin\delta_s \cdot \cos(\omega_s t) - \cos\delta_s \cdot \sin i \cdot \sin(\omega_s t)) \tag{3}$$

where i is the orbital inclination; ω_s is the angular velocity of the orbit, which can be expressed as $\omega_s = \sqrt{\frac{\mu}{(R_e+H)^3}}$; μ is a gravitational constant; H is the orbit altitude, and R_e is the average radius of the earth.

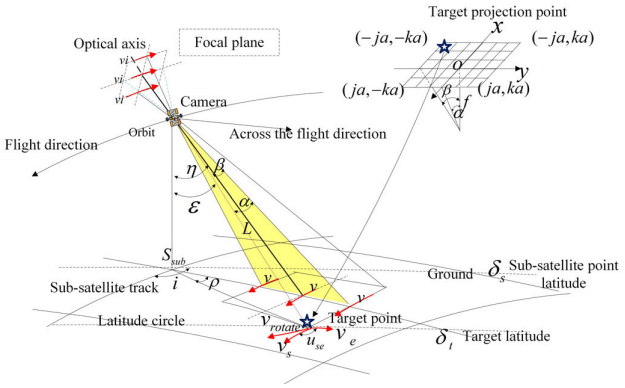

FIGURE 5. Schematic diagram of the vector relationship of the instantaneous object-image conjugate velocity fields.

2) ANALYSIS OF INSTANTANEOUS VELOCITY FIELDS

During the process of dynamic imaging, the inclination and FOV of the space camera are still unchanged. Based on the principle of ray tracing, the ground velocity of the target v is conjugated with the image velocity vi, which means the two velocities are in opposite directions, and the magnitude has a certain proportional relationship. According to these two principles, the paper first analyzes the relationship between the three velocities of the target, establishes the instantaneous velocity field on ground, and then maps the velocity vector to the focal plane to obtain the corresponding image velocity field, as shown in Fig. 5. The mathematical analysis process is as follows:

The FOV of the center of the pixel in the j row and k column along the flight direction $\alpha_{j,k}$ and across the flight direction $\beta_{j,k}$ can be described as:

$$\begin{aligned} \alpha_{j,k} &= \pm\arctan\left(\frac{j \cdot a}{\sqrt{(k \cdot a)^2 + f^2}}\right), \\ \beta_{j,k} &= \pm\arctan\left(\frac{k \cdot a}{\sqrt{(j \cdot a)^2 + f^2}}\right) \end{aligned} \tag{4}$$

where a is the pixel size, f is the camera focal length, $j = 0, 1, 2, \cdots, M$ and $k = 0, 1, 2, \cdots, N$. There are $2M+1, 2N+1$ pixels in F_1 and F_2 directions on the focal plane, respectively.

The vector heading from the center of the camera to the target center is defined as observing vector, and the vector heading from the center of the satellite to the sub-satellite center is defined as satellite-to-ground vector. Therefore, the angle $\varepsilon_{j,k}$ that between the observing vector and satellite-to-ground vector is

$$\varepsilon_{j,k} = \arccos(\cos(\eta + \beta_{j,k}) \cdot \cos(\alpha_{j,k})) \tag{5}$$

And the angle $\phi_{j,k}$ that between the direction of the earth center pointing to target and the direction of the earth center

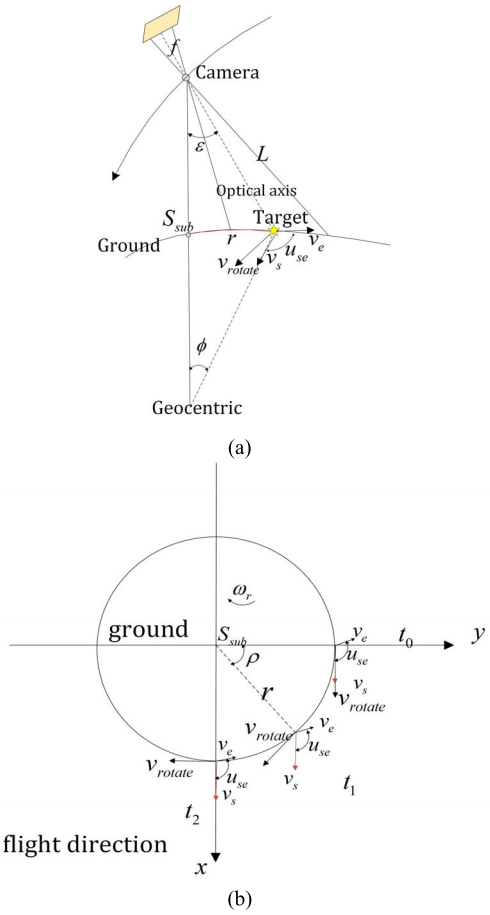

FIGURE 6. Schematic diagrams of simplified geometric model of circular scanning imaging (a) the geometric relationship between imaging parameters; (b) the geometric relationship of the three velocity vectors.

pointing to sub-satellite point is:

$$\phi_{j,k} = \arcsin(\frac{\sin(\varepsilon_{j,k}) \cdot (R_e + H)}{R_e}) - \varepsilon_{j,k} \tag{6}$$

where H represents the orbit altitude, R_e is the average radius of the earth, and the distance $L_{j,k}$ between the camera and target can be expressed as:

$$L_{j,k} = \frac{R_e \cdot \sin(\phi_{j,k})}{\sin(\varepsilon_{j,k})} \tag{7}$$

For instance, the intersection of the optical axis and the surface of earth is selected as the target point. The simplified geometric relationship between the above-mentioned imaging parameters is shown in Fig. 6 (a).

Therefore, the three velocities of the ground target that captured by the camera in a single frame are:

a) The projection of orbit precession velocity on the ground $v_{s(j,k)} = \omega_s R_e \cos\phi_{j,k}$,

b) The linear velocity of earth rotation $v_{e(j,k)} = \omega_e R_e \cos\delta_{t(j,k)}$,

c) The dynamic rotation velocity $v_{rotate(j,k)} = \omega_r \cdot L_{j,k}$.

where ω_s, ω_e, and ω_r represent the angular velocity of the orbit, the angular velocity of earth rotation, and the angular velocity of camera rotation, respectively. $\delta_{t(j,k)}$ is the latitude of the ground target, which can be expressed as:

$$\delta_{t(j,k)} = \arcsin(\sin\delta'_s \cos\phi_{j,k} + \cos\delta'_s \sin\phi_{j,k} \cos i) \tag{8}$$

where i represents the inclination of satellite orbit; and δ'_s is the latitude of sub-satellite point at different times, the initial latitude δ'_s is δ_s. $r_{j,k}$ is the radius of the circle formed by the target rotating on the ground, which can be expressed as $r_{j,k} = R_e \cdot \phi_{j,k}$.

Fig. 6 (b) shows the geometric relationship of three velocity vectors. According to this dynamic relationship, these velocities are decomposed and synthesized, and the instantaneous velocity field on the ground is obtained as:

$$v_{j,k} = \sqrt{v^2_{x_{(j,k)}} + v^2_{y(j,k)}},\ \zeta_{(j,k)} = \arctan\frac{v_{y(j,k)}}{v_{x(j,k)}} \tag{9}$$

where $v_{j,k}$ represents the value of the velocity vector; $\zeta_{(j,k)}$ is the direction of the velocity vector;$v_{x(j,k)}$ and $v_{y(j,k)}$ are the velocity components of the above three velocities in the x and y directions, can be respectively expressed as follows:

$$\begin{aligned} v_{x(j,k)} &= v_{s(j,k)} - v_{e(j,k)} \cdot \cos(\pi - u_{se(j,k)}) + v_{rotate(j,k)} \cdot \cos(\rho_{j,k}) \\ v_{y(j,k)} &= v_{e(j,k)} \cdot \sin(\pi - u_{se(j,k)}) - v_{rotate(j,k)} \cdot \sin(\rho_{j,k}) \end{aligned} \tag{10}$$

where $u_{se(j,k)}$ represents the angle between the projection velocity $v_{s(j,k)}$ and the earth rotation velocity $v_{e(j,k)}$ at different positions on the ground.

$$u_{se(j,k)} = \arccos(\frac{\cos i}{\cos\delta_{j,k}}) \tag{11}$$

And $\rho_{i,j}$ is the deflection angle of the target relative to the positive y-axis at different moments, as shown in Fig. 6(b),

$$\rho_{i,j} = \frac{\omega_r \cdot t}{\sin(\varepsilon_{i,j})}, \quad 0 \le t \le T \tag{12}$$

Finally, according to the characteristics of the optical system, the velocity components on the ground are mapped to the focal plane, and the velocity components on the focal plane can be written as:

$$\begin{bmatrix} vi_{x(j,k)} \\ vi_{y(j,k)} \end{bmatrix} = \begin{bmatrix} -\dfrac{f}{L \cdot \cos\beta_{j,k}} \\ -\dfrac{\cos(\varepsilon_{j,k} + \phi_{j,k}) \cdot f}{L_{j,k} \cdot \cos\beta_{j,k}} \end{bmatrix} \cdot \begin{bmatrix} v_{x(j,k)} \\ v_{y(j,k)} \end{bmatrix} \tag{13}$$

And the image velocity field on the focal plane, which conjugated with the velocity field on the ground denotes:

$$vi_{(j,k)} = \sqrt{vi^2_{x(j,k)} + vi^2_{y(j,k)}},\ \zeta i_{(j,k)} = \arctan\frac{vi_{y(j,k)}}{vi_{x(j,k)}} \tag{14}$$

where, vi and ζi represent the value and direction of image velocity vectors at any pixel respectively.

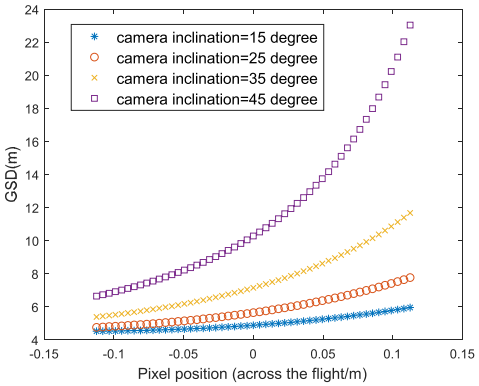

FIGURE 7. The relationship between the ground pixel resolution and the camera inclination.

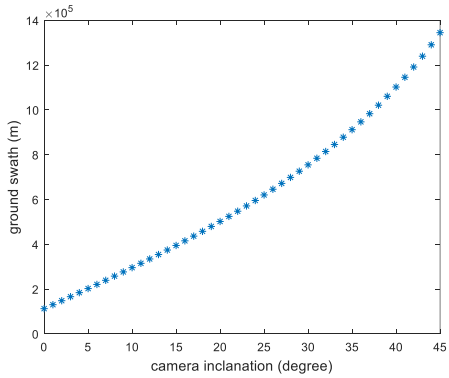

FIGURE 8. The maximum ground swath with the camera inclination.

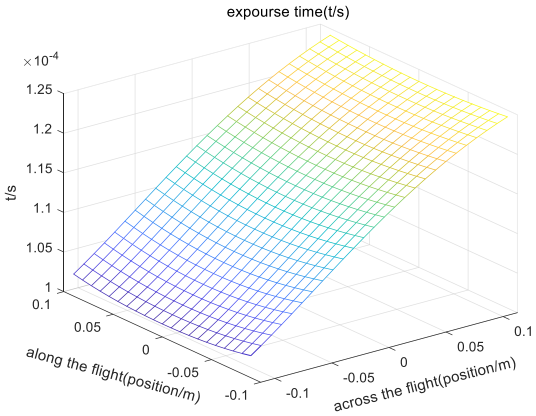

FIGURE 9. Calculation results of the exposure time at time $t = 9s$.

III. SIMULATIONS AND RESULTS

A. ANALYSIS OF CHARACTERISTICS OF THE SPACE CAMERA

Before performing the numerical and image simulations, dynamic characteristics of the space camera are analyzed from five aspects: ground pixel resolution (GSD), ground swath, image motion, modulation transfer function (MTF), and the signal-to-noise ratio (SNR) of imaging system:

1) ANALYSIS OF THE GROUND PIXEL RESOLUTION

When the space camera is imaging at a large attitude angle, the ground pixel resolution at different positions is different, also the spatial resolution is different. A calculation model of the GSD with different pixel positions is established in the direction of the vertical flight as:

$$GSD = \frac{a \cdot L_{j,k}}{f} \cdot \sec(\varepsilon_{j,k} + \phi_{j,k}) \tag{15}$$

where a represents the pixel size, f is the focal length of the camera, and $L_{j,k}$ is the distance between the camera and target. Fig. 7 are the change curves of the GSD with pixel positions at different inclinations. The ground pixel resolution increases with increasing the camera inclination and the distance, resulting in poor spatial resolution of the image. Therefore, it is necessary to balance the imaging requirements such as ground width and resolution, and reasonably design the inclination of the camera.

2) ANALYSIS OF THE GROUND SWATH

Compared with traditional sub-satellite push-broom imaging, circular scanning imaging can effectively expand the ground coverage, as shown in Fig. 1. And the ground swath mainly depends on the trajectory r covered by the camera on the ground, as shown in Fig. 6(b). To analyze the relationship between the camera inclination and the ground swath, the swath with pixel positions across the flight of the camera is expressed as:

$$SW = 2 \times R_e \times \phi_{j,k} \tag{16}$$

where R_e is the average radius of the earth, $\phi_{j,k}$ is the geocentric angle of the target. The change curve of the maximum ground swath corresponding to the pixel located at the edge of the detector with the camera inclination is shown in Fig. 8. When the camera inclination is 0°, the swath of the circular scanning imaging is the same as the swath of the sub-satellite push-broom imaging. And when the camera inclination is 35°, the swath is 8.1 times the swath of the sub-satellite push-broom imaging. The results show that the circular scanning imaging can well meet the imaging requirements of large ground swath.

3) ANALYSIS OF THE IMAGE MOTION

The image motion on the focal plane mainly depends on the exposure time of the detector, which directly determines the definition of the image. In order to obtain high-quality dynamic remote sensing images, the image motion during exposure should be less than one pixel, and the exposure time t_{int} needs to be:

$$t_{int} \leq \min(a/vi_{(j,k)}) \tag{17}$$

Fig. 9 shows the calculation results of the exposure time at time $t = 9s$. According to (17), we set the exposure time to 0.1 ms, so that the image motion of any pixel on the focal plane can be less than one pixel for circular scanning imaging.

4) ANALYSIS OF THE MTF FOR IMAGING SYSTEM

MTF can objectively evaluate the performance of the imaging system [20]. The MTF of circular scanning imaging in

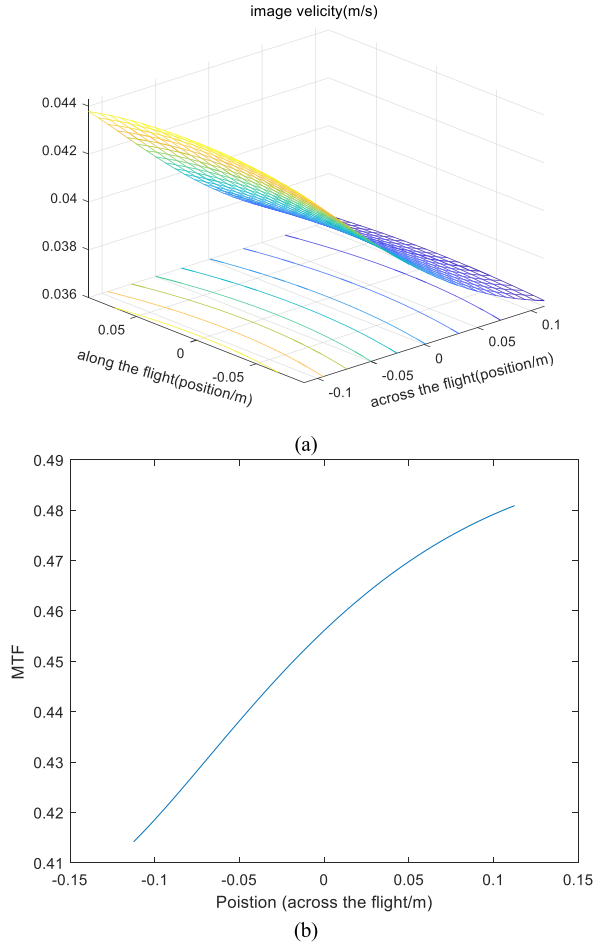

FIGURE 10. MTF of circular scanning imaging at $t = 9s$(a) image velocity of the focal plane; (b) MTF.

this paper is mainly determined by the MTF of the camera static push-broom imaging MTF_s and the MTF of the camera rotation imaging MTF_r, which can be expressed as follows:

$$MTF = MTF_s \times MTF_r = \frac{\sin(\pi \cdot a \cdot V_N)}{\pi \cdot a \cdot V_N} \times \frac{\sin\left[\frac{\pi}{2} \cdot \frac{\Delta d}{a}\right]}{\frac{\pi}{2} \cdot \frac{\Delta d}{a}} \tag{18}$$

where V_N is the Nyquist frequency, which can be expressed as $V_N = 1/2a$; Δd is the image movement distance on the focal plane during exposure, which can be expressed as $\Delta d_{(j,k)} = vi_{(j,k)} \cdot t_{int}$.

Fig. 10 shows the MTF of the image at time $t = 9s$. The faster the velocity, the larger the MTF and the worse the image quality.

5) ANALYSIS OF THE SNR FOR IMAGING SYSTEM

SNR is a key indicator for evaluating the quality of the imaging system, which reflects whether imaging parameters are suitable for high-quality imaging. The SNR of optical remote sensing imaging is expressed as follows:

TABLE 1. SNR simulation parameters.

Serial number	SNR simulation parameters	Value
1	Wavelength	400~1000nm
2	Pixel size	4.5μm
3	Transmittance of optical system	0.8
4	Exposure time	0.1ms
5	Average quantum efficiency	60%
6	F number	5.4
7	Planck constant	6.63×10-34J·s
8	Velocity of light in vacuum	3×10^8m/s
10	Dark current noise（25 centigrade）	3e-/p/s
11	Readout noise	1.6e-
12	Solar zenith angle	30°
13	Surface reflectance	0.3

$$\begin{aligned} SNR &= 20\lg \frac{N_s}{\sqrt{N_s + N_b + N_d}} \\ &= 20\lg \frac{\int_{\lambda_1}^{\lambda_2} \frac{\pi \cdot a^2 \cdot \tau \cdot \eta_{CMOS} \cdot t_{int} \cdot E(\lambda)}{4 \cdot F^2 \cdot (hc/\lambda)} d\lambda}{\sqrt{\int_{\lambda_1}^{\lambda_2} \frac{\pi \cdot a^2 \cdot \tau \cdot \eta_{CMOS} \cdot t_{int} \cdot E(\lambda)}{4 \cdot F^2 \cdot (hc/\lambda)} d\lambda + \sigma_b^2 + t_{int} \cdot \sigma_d}} (dB) \end{aligned} \tag{19}$$

where N_s, N_b and N_d are photon numbers of the shot noise σ_s, the read noise σ_b and the dark current noise σ_d of the flat-panel detector during exposure time, respectively; $E(\lambda)$ represents the solar irradiance;a is the pixel size of the detector;τ represents the transmittance of the optical system; η_{CMOS} is the average quantum efficiency of the detector; t_{int} is the exposure time;F is the F number of the optical system; h is the Planck constant; c is the velocity of light in vacuum and λ is the wavelength of light.

Table 1 shows parameters for SNR simulation. According to (19), the SNR of the imaging system is calculated about 30dB, which can meet the practical application needs for remote sensing imaging of space cameras.

B. NUMERICAL SIMULATION AND RESULTS OF INSTANTANEOUS VELOCITY FIELDS

Numerical simulation is carried out to analyze the dynamic characteristics of the space camera which performs circular scanning imaging. According to the actual imaging requirements, Table 2 gives the numerical simulation parameters. It can be seen that the number of pixels in vertical flight direction is more than that in the flight direction, so the two adjacent frames in the vertical flight direction can be seamlessly stitched, realizing the expansion of the circular scanning imaging area.

TABLE 2. Numerical simulation parameters.

Serial number	Numerical simulation parameters	Value
1	Satellite orbit inclination	97°
2	Camera focal length	0.5m
3	Camera pixel size	4.5um
4	Orbit altitude	500km
5	Latitude of sub-satellite point at time t_0	30°
6	The camera inclination	35°
7	The time for the camera to make one revolution	36s
8	Camera rotation angular velocity	5.7358°/s
10	The number of pixels in the flight direction	40000pixels
11	The number of pixels in the vertical flight direction	50000pixels

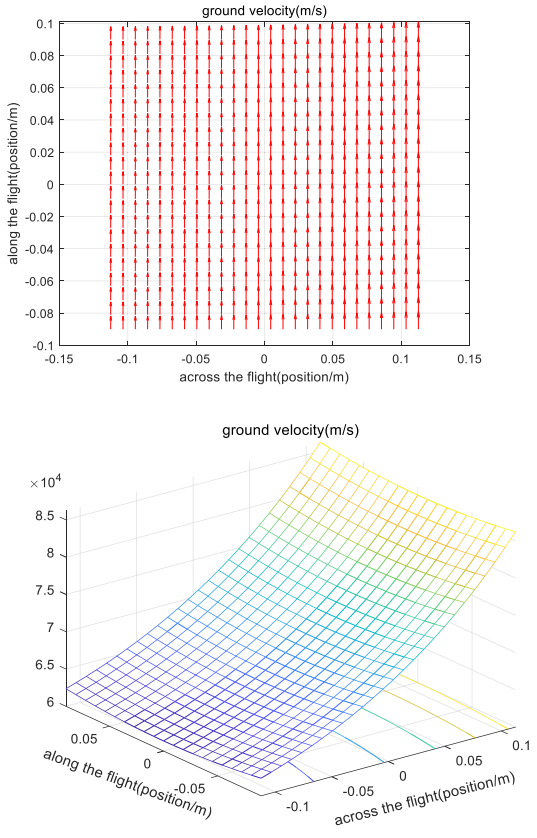

FIGURE 11. Velocity filed distribution on ground and velocity change curve at $t = 0s$.

Because there is no relative movement between the satellite platform and the camera, the yaw attitude angular velocity is identical to the camera rotation angular velocity. According to (9) and (14), combined with imaging parameters in Table 1, the numerical simulation results of the distribution of the instantaneous velocity fields at different times are shown in Fig. 11 to Fig. 16, respectively.

Through the analysis of numerical simulations, the following results can be obtained:

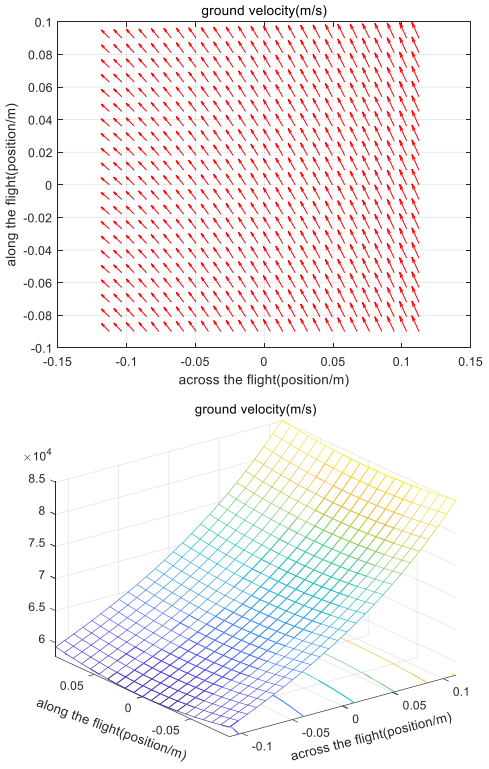

FIGURE 12. Velocity filed distribution on ground and velocity change curve at $t = 4s$.

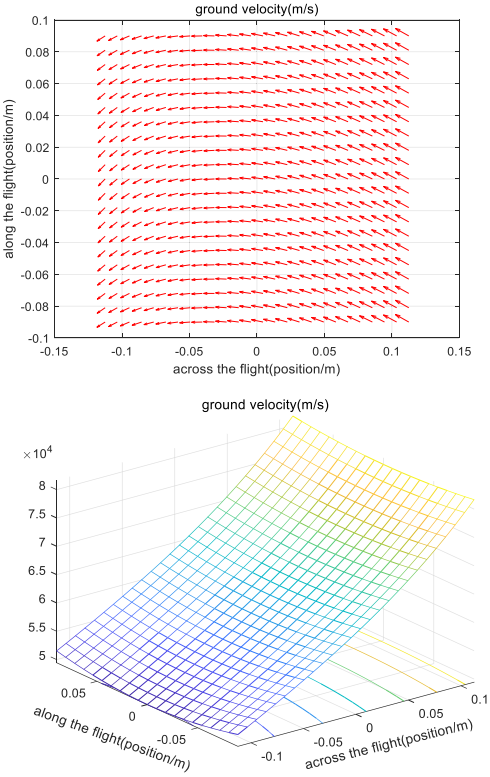

FIGURE 13. Velocity filed distribution on ground and velocity change curve at $t = 9s$.

1) The instantaneous velocity fields are nonlinearly changed affected by the curvature of the earth: At time $t = 9s$,

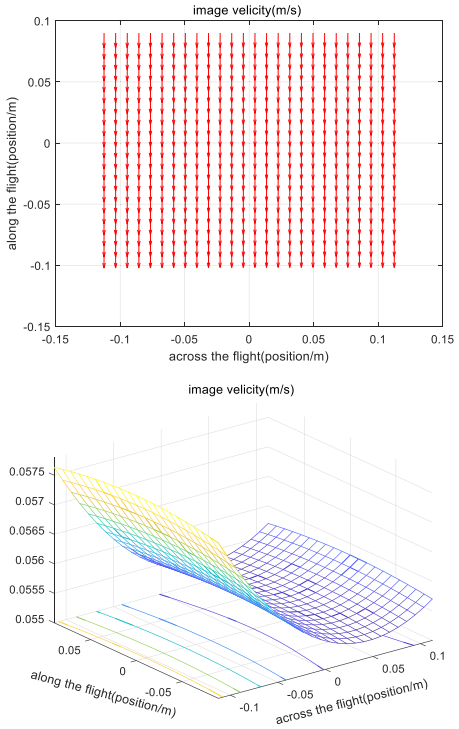

FIGURE 14. Image velocity filed distribution on the focal plane and velocity change curve $t = 0s$.

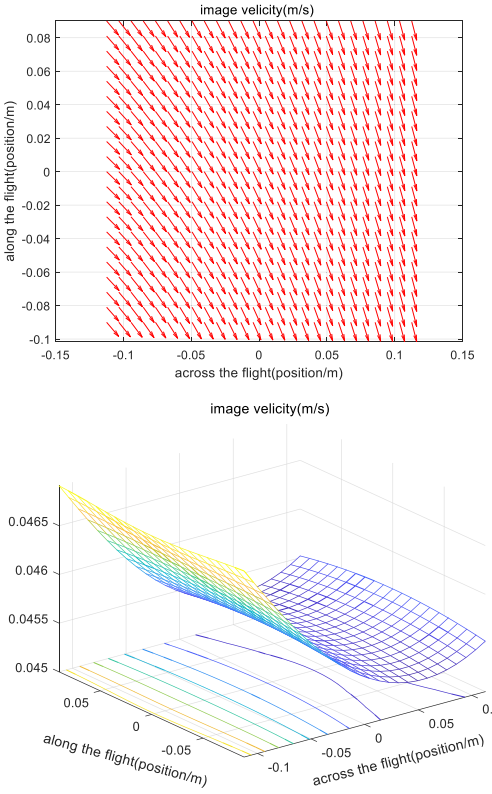

FIGURE 15. Image velocity filed distribution on the focal plane and velocity change curve $t = 4s$.

the maximum ground velocity is 80km/s and the minimum is 50km/s. Due to the vector mapping relationship between the

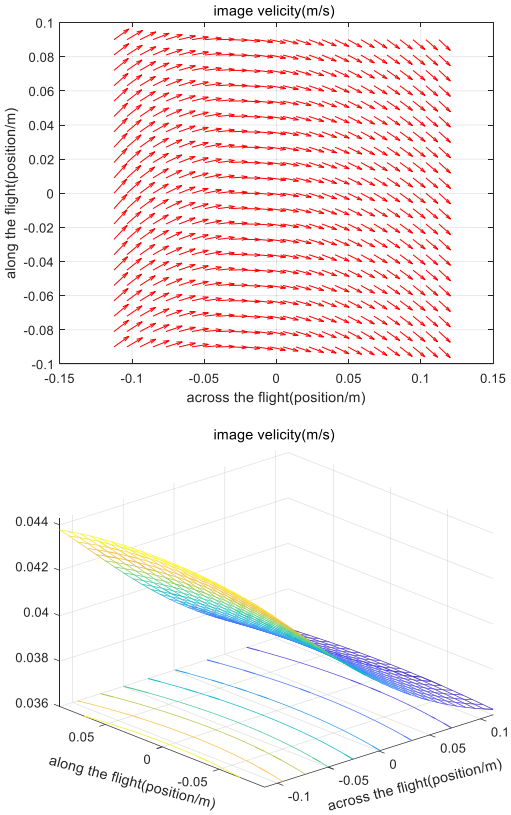

FIGURE 16. Image velocity filed distribution on the focal plane and velocity change curve $t = 9s$.

image velocity on the focal plane and the ground velocity, the maximum image velocity is 0.04m/s and the minimum is 0.036m/s;

2) The instantaneous velocity fields show anisotropic distribution, as shown in Fig. 11 $\sim$ Fig. 16. For instance, at time $t = 9s$, the velocity vector is affected by the rotation motion, which deviates from the flight direction by a maximum angle of 80 degree and a minimum angle of 50 degree;

3) The dynamic characteristics of space cameras have different effects on the imaging quality. Therefore, it is necessary to balance the imaging parameters to ensure the imaging quality. The quantitative analyses show that the greater the dynamic velocity and the longer the exposure time, resulting in the worse imaging quality.

When the exposure time is 0.1ms, the SNR of the imaging system is about 30dB, the image motion of each pixel is less than one pixel, and the image PSNR is about 29dB, which basically meets the imaging requirements.

C. IMAGE SIMULATION OF CIRCULAR SCANNING IMAGING

1) IMAGE SIMULATION

To intuitively observe the effect of the circular scanning imaging, remote sensing images are used for imaging simulation, and the simulation process is as follows: First of all, the remote sensing panchromatic image is processed for geometric sampling, and the red area is the simu-

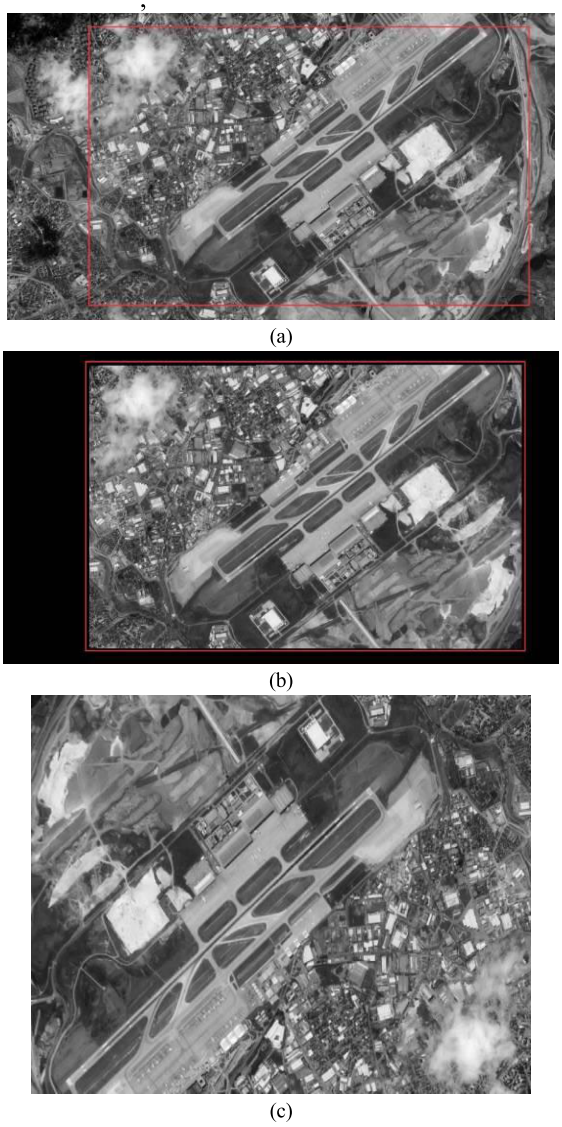

FIGURE 17. Simulation process for circular scanning imaging. (a) real-scene image; (b) simulated instantaneous ground image; (c) simulated instantaneous focal plane image.

lated trapezoid image in a single frame at a large attitude angle, as shown in Fig.17 (a); Next, the instantaneous ground velocity field at time $t = 9s$ is added to the real-scene image, and the instantaneous ground simulated image with an exposure time of 0.1ms is obtained, as shown in Fig.17 (b); Finally, a resolution inversion method [21] is performed on the ground simulation image to obtain the instantaneous focal plane simulation image which conjugated with the ground simulation image, as shown in Fig. 17 (c).

2) ANALYSIS OF THE PSNR FOR SIMULATED IMAGES

PSNR is the most widely used objective criterion for processed images [22]. It can measure the simulation image of circular scanning imaging at different exposure times, clearly reflecting the comparison with the standard image.

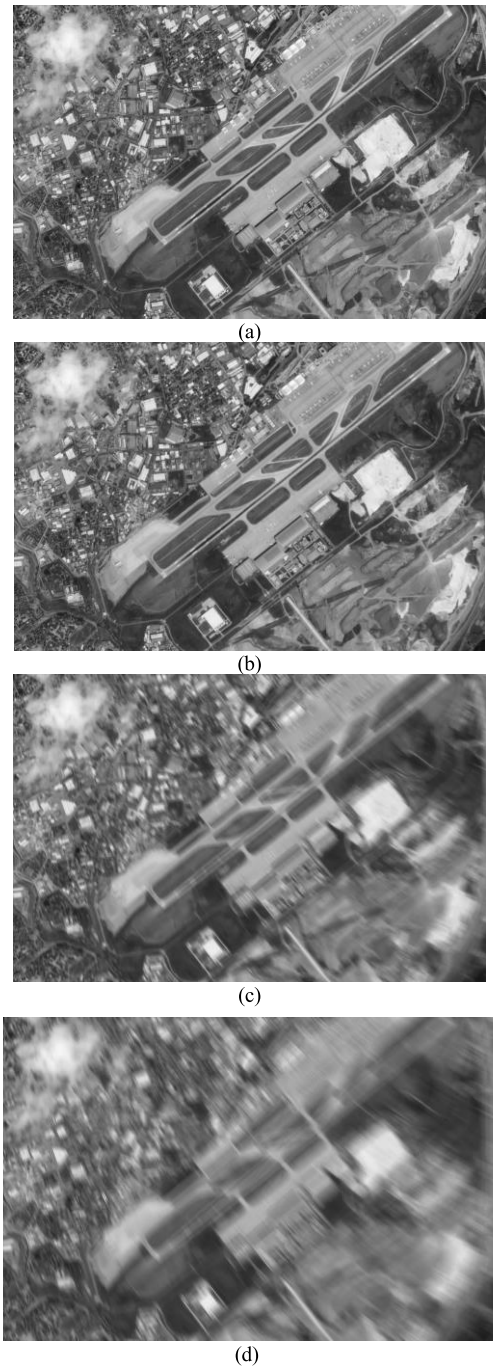

FIGURE 18. Simulation results of different exposure times. (a) Image without image motion; (b) $t_{int} = 0.1ms$, PSNR 28.89; (c) $t_{int} = 1ms$, PSNR=24.31; (d) $t_{int} = 10ms$, PSNR=20.17.

Also, PSNR is based on the error between the pixels of the processed and standard images, therefore it is selected to evaluate simulated images in this paper. The definition of PSNR can be expressed as follows:

$$PSNR=20 \times \lg(\frac{255}{\sqrt{MSE}}) \tag{20}$$

where MSE is the mean square error between the simulated image $I(j, k)$ and the real-scene image $K(j, k)$, which can be

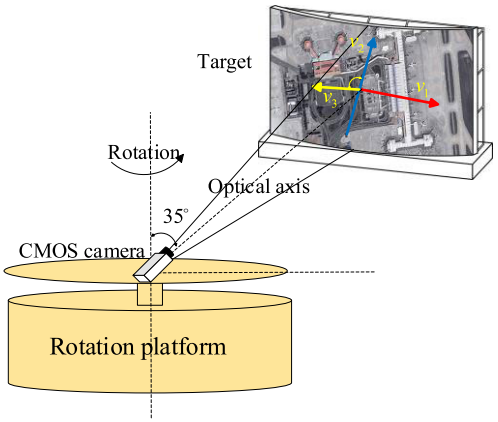

FIGURE 19. Sketch diagram of the ground experiment for circular scanning imaging.

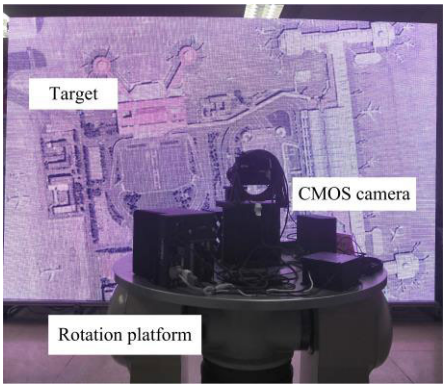

FIGURE 20. Ground experiment equipment of circular scanning imaging.

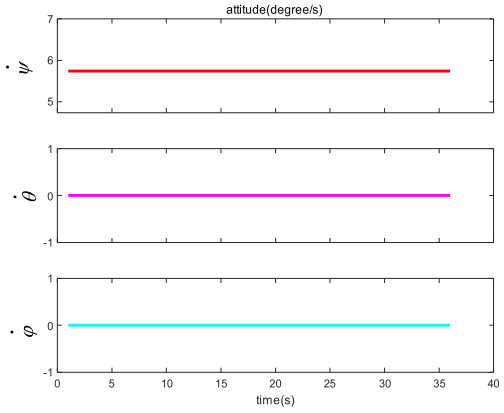

FIGURE 21. The attitude angular velocity of the rotation platform.

expressed as follows:

$$MSE = \frac{1}{(2M+1)(2N+1)} \sum_{j=1}^{2M+1} \sum_{k=1}^{2N+1} \|I(j,k) - K(j,k)\|^2 \tag{21}$$

Fig. 18 shows the simulated images at different exposure times and the corresponding PSNR. The longer the exposure time, the smaller the PSNR, resulting in the poorer image quality. Therefore, it is necessary to set the detector exposure

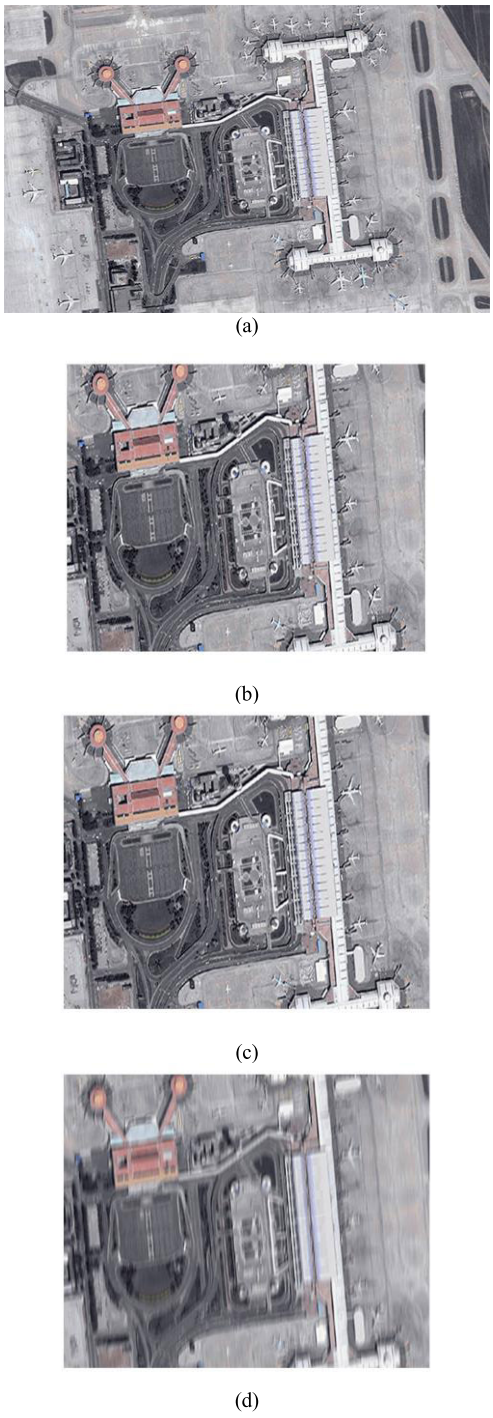

FIGURE 22. The experimental images of circular scanning imaging (a) target; (b)experimental image at 0.1ms; (c) experimental image at 1ms; (d) experimental image at 10ms.

time reasonably to ensure the imaging quality of the circular scanning imaging.

D. GROUND EXPERIMENT

1) GROUND EXPERIMENT OF CIRCULAR SCANNING IMAGING

A ground experiment was made to evaluate the analysis of imaging velocity fields proposed by this paper. Fig. 19 shows

TABLE 3. PSNR for simulated and experimental images.

	0.1ms	1ms	10ms
Simulated images	28.89dB	24.31 dB	20.17 dB
Experimental images	24.34 dB	22.21 dB	17.38 dB

the principle diagram of the ground experiment for circular scanning. In the experiment, v_1 is the velocity generated on the target by the rotation of the turntable, which corresponds to the dynamic rotation velocity of circular scanning imaging v_{rotate}; v_2 is the velocity of the target moving, which corresponds to the projection of orbit precession velocity on the ground v_s; and v_3 corresponds to the linear velocity of earth rotation v_e.

The ground experiment equipment for circular scanning imaging is shown in Fig. 20. The experiment system mainly includes a rotation platform, a high-resolution CMOS camera and a large target [2]. Where the platform simulates the satellite to provide attitude, the large target simulates the target on the ground, and the CMOS camera is tilted at 35° and fixed on the turntable to simulate circular scanning imaging. The pixel size of CMOS camera is 4.5μm; the focal length of the camera is 0.5mm; and the size of the large target is 6m×4m.

The precision of the rotation platform for the ground experiment is 0.001 °/s, and the attitude angular velocity during the imaging process is shown in Fig. 21. Since the rotation velocity of the camera is the main reason for the anisotropic distribution of the imaging velocity, the yaw velocity of the turntable is controlled to 5.7358 °/s corresponding to the model of the circular scanning imaging.

2) EXPERIMENT RESULTS

The experimental images are obtained by changing the exposure time of the CMOS camera as shown in Fig. 22. The PSNR of experimental images are 24.34 dB, 22.21 dB, 17.38 dB respectively. As shown in Table 3, the experimental results are different from the simulation results due to the moving parts such as fiber optic gyroscope and reaction flywheel in the ground experiment system, it still proves the correctness of the velocity field model in this paper.

IV. CONCLUSION

In this paper, a mathematical model of the velocity field for circular scanning imaging is proposed to evaluate the image quality. The mathematical model of the ground velocity field is firstly established based on the principle of ray tracing; and then according to the conjugate correspondence between pixels and targets, the image velocity field on the focal plane is obtained. The numerical simulations result show that the velocity vector is anisotropic at different times. The analyses of the dynamic characteristics and the effect of circular scanning imaging show that the longer the exposure time, the faster the velocity, and result in worse image quality. In short, the space camera with the static-dynamic transformation can perform a new circular scanning model. This mode can effectively expand the imaging area and obtain high-resolution images. However, the changing velocity of this mode will have a serious impact on the image. Therefore, it is necessary to balance the relationship between the imaging parameters. We hope that the study in this paper is useful for analyzing the effect of dynamic imaging velocity on imaging quality.

REFERENCES

[1] W. Y. Li, C. H. Hu, and L. Zhang, "Drift angle compensation method for a high-resolution, wide-range space camera," *Meas.*, vol. 158, p. 11, Jul. 2020.
[2] C. Xu, X. B. Yang, and T. T. Xu, "Study of space optical dynamic push-broom imaging along the trace of targets," *Optik*, vol. 202, Feb. 2020, Art. no. 163640.
[3] R. L. Pu, S. Landry, and Q. Y. Yu, "Assessing the potential of multi-seasonal high resolution Pléiades satellite imagery for mapping urban tree species," *Int. J. Appl. Earth Observ. Geoinf.*, vol. 71, pp. 144–158, Sep. 2018.
[4] M. Alkan, G. Buyuksalih, U. G. Sefercik, and K. Jacobsen, "Geometric accuracy and information content of WorldView-1 images," *Opt. Eng.*, vol. 52, no. 2, Feb. 2013, Art. no. 026201.
[5] F. de Lussy, D. Greslou, and C. Dechoz, "Pleiades hr in flight geometrical calibration: Location and mapping of the focal plane," in *XXII ISPRS Congress, Technical Commission I, International Archives of the Photogrammetry Remote Sensing and Spatial Information Sciences*, M. Shortis and N. ElSheimy, Eds. Göttingen, Germany: Copernicus Gesellschaft Mbh, 2012, pp. 519–523.
[6] W. Qiu and C. Xu, "Attitude maneuver planning of agile satellites for time delay integration imaging," *J. Guid., Control, Dyn.*, vol. 43, no. 1, pp. 46–59, Jan. 2020.
[7] B. Yang, M. Wang, and S. Y. Jin, "An optimal imaging-scheduling algorithm for the multi-strip imaging-mode of the high-resolution agile satellites based on certain step-size search," in *XXII ISPRS Congress, Technical Commission I, International Archives of the Photogrammetry Remote Sensing and Spatial Information Sciences*, M. Shortis N. ElSheimy, Eds. Göttingen, Germany: Copernicus Gesellschaft Mbh, 2012, pp. 339–343.
[8] Y. Xu, J. W. Chen, and Y. T. Chen, "Geometric simulation analysis of multi-band mosaic imaging from the same orbit by agile satellites," in *Remote Sensing of the Environment* Q. Tong and B. Zhu, Eds. Bellingham, WA, USA: Spie-Int Soc Optical Engineering, 2015.
[9] M. Lemaître, G. Verfaillie, F. Jouhaud, J.-M. Lachiver, and N. Bataille, "Selecting and scheduling observations of agile satellites," *Aerosp. Sci. Technol.*, vol. 6, no. 5, pp. 367–381, Sep. 2002.
[10] D. Ye, H. Z. Zhang, and Y. X. Tian, "Fuzzy sliding mode control of nonparallel-ground-track imaging satellite with high precision," *Int. J. Control, Automat. Syst.*, vol. 18, pp. 1617–1628, Jan. 2020.
[11] D. Wu, Y. Chen, Q. Li, Z. Xu, H. Feng, and Y. Man, "Attitude scheduling and verification for dynamic imaging of agile satellites," *Optik*, vol. 206, Mar. 2020, Art. no. 164365.
[12] X. B. Cao, F. Wang, and H. Y. Li, "An ultra-wide range circular scanning imaging method of optical satellite," Chinese Patent CN108 151 711 A, Jun. 12, 2018.
[13] M. Song, H. Qu, and G. Zhang, "Design of aerospace camera circular scanning imaging model," *Infr. Laser Eng.*, vol. 47, no. 7, 2018, Art. no. 0718001.
[14] S. Roques, L. Jahan, B. Rouge, *Satellite Attitude Instability Effects on Stereo Images*, New York, NY, USA: IEEE Press, 2004.
[15] B. M. Miller and E. Y. Rubinovich, "Image motion compensation at charge-coupled device photographing in delay-integration mode," *Autom. Remote Control*, vol. 68, no. 3, pp. 564–571, Mar. 2007.
[16] H. J. Zhao, H. Shang, and G. R. Jia, "Simulation of remote sensing imaging motion blur based on image motion vector field," *J. Appl. Remote Sens.*, vol. 8, p. 13, Oct. 2014.
[17] Q. Huang, F. Yang, and J. Zhao, "Drift angle analysis for agile satellite imaging when its attitude points to the earth changing continuously," *J. Chin. Soc. Astronaut.*, vol. 33, no. 10, pp. 1544–1551, 2012.
[18] C. Wang, Z. You, and F. Xing, "Image motion velocity field for wide view remote sensing camera and detectors exposure integration control," *Acta Optica Sinica*, vol. 33, no. 5, 2013, Art. no. 0511002.

[19] J. Wang, P. Yu, and C. Ya, "Space optical remote sensor image motion velocity vector computational modeling," *Acta Optica Sinica*, vol. 24, no. 12, pp. 1585–1589, 2004.
[20] Y. Xiubin, H. Xiaojun, and Z. Liu, "Effect and simulation of the deviant angle error on TDI CCD cameras image," *Opto-Electron. Eng.*, vol. 35, no. 11, p. 45, 2008.
[21] C. Xu, G. Jin, and X. Yang, "Inversion restoring algorithm for whiskbroom scanning images synthesized with deep convolutional neural network," *Acta Optica Sinica*, vol. 39, no. 12, 2019, Art. no. 1228001.
[22] J. Korhonen and J. You, "Peak signal-to-noise ratio revisited: Is simple beautiful?" in *Proc. 4th Int. Workshop Qual. Multimedia Exper.*, Jul. 2012, pp. 37–38.

TINGTING XU received the B.Eng. degree in opto-electronics information science and engineering from Sichuan University, Chengdu, China, in 2017. She is currently pursuing the Ph.D. degree in optical engineering with the Changchun Institute of Optics, Fine Mechanics, and Physics, Chinese Academy of Sciences. Her research interests include optical design and dynamic optical remote sensing imaging.

XIUBIN YANG received the B.S. degree in physics from the University of NanKai, Tianjin, in 2006, and the Ph.D. degree in optical engineering from the Chinese Academy of Sciences, Changchun, in 2011. He is currently a Professor with the Department of Space New Technique, Changchun Institute of Optics, Fine Mechanics, and Physics, Chinese Academy of Sciences. His research interests include the dynamic imaging process of space optical camera, the new mode of optical imaging, and advanced optical payload technology.

SHAOEN WANG received the B.S. degree from the Harbin Institute of Technology, Weihai, China, in 2019. He is currently pursuing the M.S. degree with the Changchun Institute of Optics, Fine Mechanics, and Physics, Chinese Academy of Sciences. His research interests include dynamic imaging and image processing.

JINLIANG HAN received the B.Eng. degree in electronic information science and technology from Xiamen University, Xiamen, China, in 2018. He is currently pursuing the M.S. degree in optical engineering with the Changchun Institute of Optics, Fine Mechanics, and Physics, Chinese Academy of Sciences. His research interests include dynamic optical imaging and super-resolution imaging.

LIN CHANG received the B.S. degree in physics from the University of Nankai, Tianjin, in 2009, and the Ph.D. degree in optical engineering from the Chinese Academy of Sciences, Changchun, in 2014. She is currently an Associate Professor with the Department of Space New Technique, Changchun Institute of Optics, Fine Mechanics, and Physics, Chinese Academy of Sciences. Her research interests include satellite attitude control and the imaging of space optical cameras.

WEI YUE received the B.Eng. degree in measurement control technology and instruments from the Changchun University of Science and Technology, Changchun, China, in 2018. She is currently pursuing the M.S. degree in optical engineering with the Changchun Institute of Optics, Fine Mechanics, and Physics, Chinese Academy of Sciences. Her research interests include dynamic optical imaging and optical design.